

## Multirhythmic bursting

Robert J. Butera, Jr.<sup>a)</sup>

*Mathematical Research Branch, National Institute of Diabetes and Digestive and Kidney Diseases, National Institutes of Health, 9190 Wisconsin Avenue, Suite 350, Bethesda, Maryland 20814*

(Received 24 July 1997; accepted for publication 20 October 1997)

A complex modeled bursting neuron [C. C. Canavier, J. W. Clark, and J. H. Byrne, *J. Neurophysiol.* **66**, 2107–2124 (1991)] has been shown to possess seven coexisting limit cycle solutions at a given parameter set [Canavier *et al.*, *J. Neurophysiol.* **69**, 2252–2259 (1993); **72**, 872–882 (1994)]. These solutions are unique in that the limit cycles are concentric in the space of the slow variables. We examine the origin of these solutions using a minimal 4-variable bursting cell model. Poincaré maps are constructed using a saddle-node bifurcation of a fast subsystem such as our Poincaré section. This bifurcation defines a threshold between the active and silent phases of the burst cycle in the space of the slow variables. The maps identify parameter spaces with single limit cycles, multiple limit cycles, and two types of chaotic bursting. To investigate the dynamical features which underlie the unique shape of the maps, the maps are further decomposed into two submaps which describe the solution trajectories during the active and silent phases of a single burst. From these findings we postulate several necessary criteria for a bursting model to possess multiple stable concentric limit cycles. These criteria are demonstrated in a generalized 3-variable model. Finally, using a less direct numerical procedure, similar return maps are calculated for the original complex model [C. C. Canavier, J. W. Clark, and J. H. Byrne, *J. Neurophysiol.* **66**, 2107–2124 (1991)], with the resulting mappings appearing qualitatively similar to those of our 4-variable model. These multistable concentric bursting solutions cannot occur in a bursting model with one slow variable. This type of multistability arises when a bursting system has two or more slow variables and is viewed as an essentially second-order system which receives discrete perturbations in a state-dependent manner. [S1054-1500(98)02001-1]

**Autonomous bursting systems are characterized by periods of repetitive activity punctuated by periods of quiescence. Physical examples of such systems include the Belousov–Zhabotinsky-reaction and electrically excitable cells, such as pancreatic  $\beta$ -cells and neuron R15 in the abnominal ganglion of the aquatic mollusc *Aplysia*, or sea hare. Recent studies<sup>2,3</sup> of a model of neuron R15<sup>1</sup> have shown that at certain parameter ranges the model possesses as many as eight stable coexisting periodic bursting solutions. This is by far the most extreme example of multirhythmicity in an autonomous system. We develop a technique to locate these regions of multirhythmicity and investigate the nature of these solutions in a simple model of an excitable bursting cell. The origin of the multirhythmicity is hypothesized and demonstrated in a general model as well as a more complex bursting model.<sup>1</sup> It is possible that other bursting systems with at least two slow variables may possess regions of parameter space with similar types of multiple bursting solutions.**

### I. INTRODUCTION

A variety of neural preparations exhibit the phenomenon of *birhythmicity*: the coexistence of two stable periodic solutions without any changes in the parameters of the dynamical system. These solutions may be switched between by a brief

transient input, such as an externally applied current pulse. Experimental examples include bursting and beating states in invertebrate neurons<sup>4,5</sup> and two spiking states (with different frequencies) in turtle motoneurons.<sup>6</sup> Several of these examples have also been the subject of theoretical studies.<sup>7,8</sup> Birhythmicity has also been demonstrated in a variety of modeled biochemical systems.<sup>9</sup> We distinguish birhythmicity from the more general *bistability*: the coexistence of two stable solutions, where typically one solution is at equilibrium and the other is periodic. There are many neuronal models which exhibit bistability.<sup>10</sup>

More recent theoretical studies have provided examples of model systems that possess three or more stable coexisting oscillatory states, also known as *multirhythmicity*. Three coexisting oscillatory states have been demonstrated in a modeled biochemical system.<sup>11</sup> Multirhythmicity has also been demonstrated in both integrate-and-fire and Hodgkin–Huxley neural models with delayed feedback.<sup>12</sup> Canavier *et al.*<sup>2,3</sup> have demonstrated possibly the most intriguing notion of multirhythmicity in an autonomous system. In their studies of a model of neuron R15 in *Aplysia*,<sup>1</sup> it was found that within certain parameter regimes the model possessed as many as eight coexisting oscillatory solutions. These solutions could be switched between by an appropriately timed input stimulus and were unique in that the limit cycles were concentric in the state space of the two slow variables.

In this study we seek to address the origin of the multistable periodic solutions demonstrated by Canavier *et al.*<sup>2</sup>

<sup>a)</sup>Electronic mail: butera@helix.nih.gov

We believe that this form of multirhythmicity arises from properties unique to a specific class of bursting systems, and refer to it as *multirhythmic bursting*. This paper is organized as follows. We start by introducing a minimal 4-variable bursting neuron model based on a mechanism of bursting similar to the model of Canavier *et al.*<sup>1</sup> Recent work on the geometry of the solution space of modeled bursting neurons is reviewed,<sup>13,14</sup> and we define a one-dimensional return map based on this geometry. We illustrate the existence of four coexisting bursting solutions in our model using our return maps. Numerical computations of the one-dimensional return map and its decomposition into two submaps provide several insights into the origin of multirhythmic bursting. Minimal mechanisms are proposed by which a bursting system exhibits multirhythmicity, and these mechanisms are demonstrated in a general 3-variable dynamical system. Finally, a related method of generating one-dimensional return maps is applied to the model of Canavier *et al.*<sup>1</sup> The bursting solutions portrayed in Canavier *et al.*<sup>2</sup> are identified and it is shown that their model possesses a one-dimensional return map that is qualitatively similar to the map derived from our minimal model.

## II. A MINIMAL BURSTING MODEL

The endogenously bursting neuron R15 in *Aplysia* has been modeled extensively,<sup>15,7,1,16,13</sup> building upon over 40 years of electrophysiological investigations.<sup>17</sup> The model presented here is not intended to be a complete physiological model. Rather, we wished to develop the simplest model possible which captured the essential dynamics of the more complex model of Canavier *et al.*<sup>1</sup>

Our model consists of only four ionic currents.  $I_{Na}$  and  $I_K$ , the fast  $Na^+$  and delayed-rectifier  $K^+$  currents, are responsible for the generation of action potentials. Bursting occurs via  $I_{SI}$ , a  $Ca^{2+}$  current that is activated by a slow voltage-dependent variable and inactivated by intracellular  $Ca^{2+}$ . This current is opposed by  $I_L$ , a  $K^+$  leakage current. The differential equations of the model are

$$\dot{V} = I_{Na}(V) + I_K(V, w) + I_{SI}(V, s, c) + I_L(V) - I_{app}, \quad (1)$$

$$\dot{w} = \phi_w(w_\infty(V) - w) / \tau_w(V), \quad (2)$$

$$\dot{s} = (s_\infty(V) - s) / \tau_s, \quad (3)$$

$$\dot{c} = -k_{Na}I_{Na}(V) - k_{SI}I_{SI}(V, s, c) - k_c c. \quad (4)$$

The change in membrane potential  $V$  is proportional to the sum of the ionic fluxes across the membrane, assuming that the neuron is isopotential. All conductances have been normalized to the capacitance of the cell membrane, which does not appear as a parameter in the model. Action potentials are generated by the fast  $Na^+$  and  $K^+$  currents, based on the minimal model of Morris and Lecar.<sup>18,19</sup> The variables  $w$  and  $s$  represent the voltage-dependent inactivation of  $I_K$  and voltage-dependent activation of  $I_{SI}$ , respectively. The change in concentration of intracellular  $Ca^{2+}$ ,  $c$ , is due to influx via  $Ca^{2+}$  currents and efflux via  $Ca^{2+}$  diffusion and extrusion. The model of Canavier *et al.*<sup>1</sup> explicitly models a fast  $Ca^{2+}$  current which is responsible for a rapid influx of

$Ca^{2+}$  associated with each action potential. To keep our model simple we did not explicitly model this current. Rather, we introduced a term into Eq. (4),  $k_{Na}$ , which dynamically achieves a similar effect, since the dynamics of  $I_{Na}$  are such that it is activated briefly but strongly with each action potential.

## III. COMPUTATIONAL METHODS

All numerical simulations of our minimal cell model use the parameter set in the Appendix, with  $\tau_s$  indicated in the text for each simulation. Simulations of the model of Canavier *et al.*<sup>1</sup> utilize the model as published with  $I_{STIM} = 1.3$  nA.

Software for numerical simulations was developed on Pentium or RS/6000 based Linux or UNIX workstations. Temporal numerical integration of solution trajectories was accomplished with software written in C and utilizing the numerical integration package CVODE.<sup>20</sup> CVODE may be obtained from <http://netlib.cs.utk.edu/ode/cvode.tar.Z>. Bifurcation diagrams were computed using the interactive ordinary differential equation simulation package XPP, which has an interface to the bifurcation analysis software package AUTO.<sup>21</sup> XPP is available at <ftp://ftp.math.pitt.edu/pub/bardware>.

## IV. THE GEOMETRY OF BURSTING

Rinzel<sup>22</sup> introduced a geometric approach toward analyzing the solution of models of bursting cells with a single slow variable. This work was extended by Rinzel and Lee<sup>13</sup> to consider bursting models with two slow variables.

A typical limit cycle oscillation for Eqs. (1)–(4) is shown in Figs. 1(A1)–(A3). Our analysis exploits the fact that two variables operate on a time scale much slower than the remaining variables of the model.  $V$  and  $w$  vary over a time scale of milliseconds, while  $c$  and  $s$  vary over a time scale of seconds and hundreds of milliseconds, respectively. We refer to the FAST subsystem as Eqs. (1) and (2) with  $c$  and  $s$  treated as parameters. Our analysis further exploits that fact that  $c$  and  $s$  parametrize the FAST subsystem via a single functional expression

$$g_{SI}(c, s) = \bar{g}_{SI} s / (1 + \beta c), \quad (5)$$

where  $g_{SI}$  is the conductance of  $I_{SI}$ . We will refer interchangeably to the FAST subsystem as parametrized one dimensionally by  $g_{SI}$  or two dimensionally by  $(c, s)$ . A bifurcation analysis of the FAST system is illustrated in Fig. 1(B1). For low values of  $g_{SI}$ , the FAST system has a stable equilibrium solution defining a manifold  $VSS$ . At larger values of  $g_{SI}$ , the FAST system possesses a stable oscillatory solution manifold  $AP$ . This manifold begins at a Hopf bifurcation and terminates at the knee of the equilibrium solution branch where  $g_{SI} = g_{HC}$ .  $g_{HC}$  denotes the location of a homoclinic saddle-node bifurcation and defines the boundary between the  $VSS$  and  $AP$  manifolds.

Figure 1(B2) is a close-up view of the boxed area of Fig. 1(B1) and illustrates the superposition of the solution trajectory of the full system [Eqs. (1)–(4)] in the  $(g_{SI}, V)$  plane. Figure 1(C) illustrates  $VSS$  and the solution trajectory in

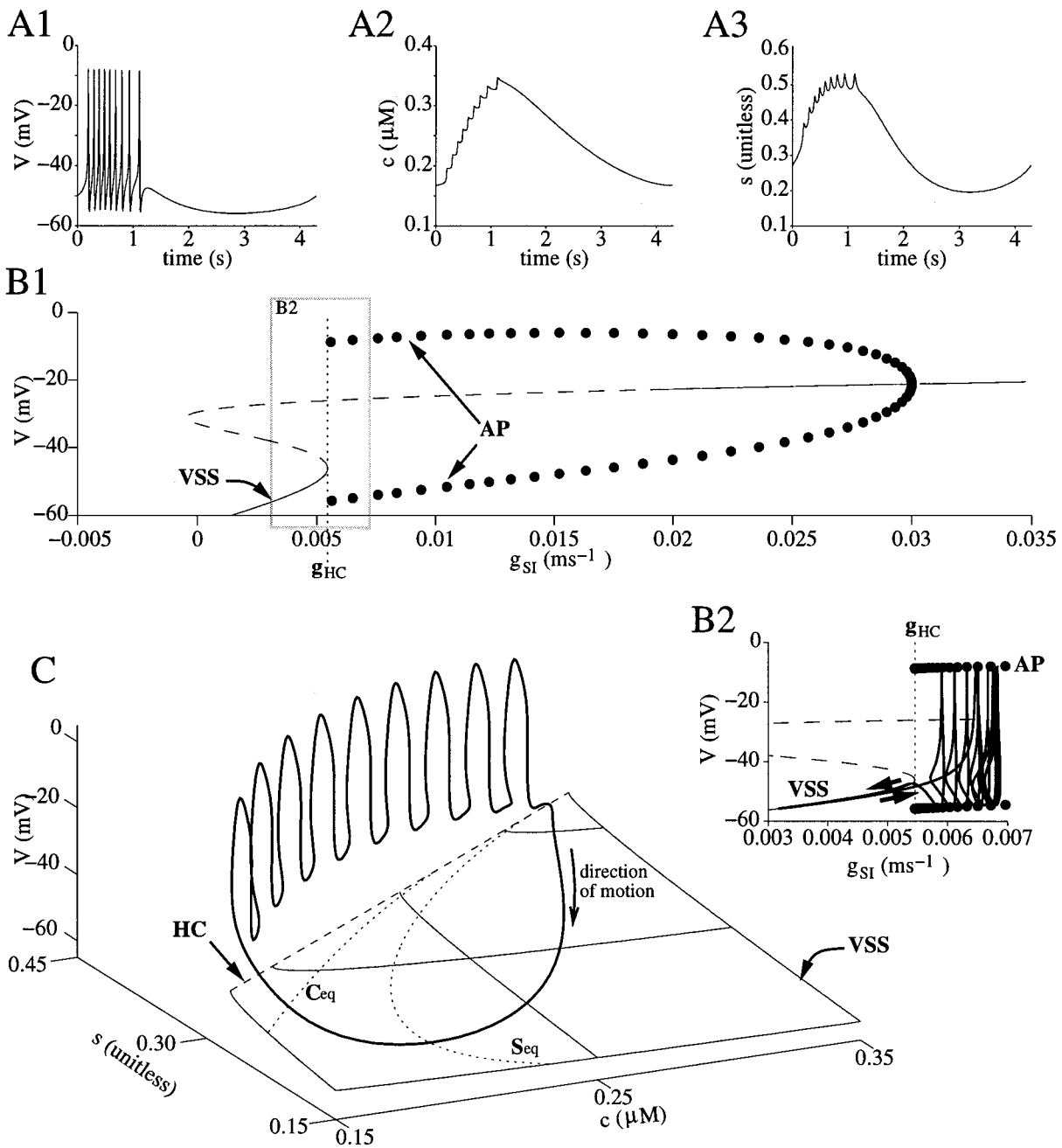


FIG. 1. Bifurcation analysis of bursting limit cycle. (A1)–(A3). Membrane potential, intracellular  $\text{Ca}^{2+}$  concentration, and voltage-dependent activation of  $I_{S1}$ , respectively. (B1). Bifurcation analysis of Eqs. (1) and (2) as  $g_{S1}$  (a function of  $c$  and  $s$ ) is varied. Stable equilibrium solutions represented by solid lines; unstable equilibrium solutions by dashed lines. The periodic solution branch emanates from a Hopf bifurcation and is represented by the minimum and maximum of the oscillation (open circles). The hyperpolarized equilibrium solution branch and periodic solution branch are labeled VSS and AP, respectively. (B2). Blown-up inset of panel (B1). Solution trajectory in terms of  $g_{S1}(c,s)$  and  $V$  is superimposed. (C). Solution trajectory in  $(c,s,V)$  space. VSS surface indicated by solid lines,  $HC(g_{HC}(c,s))$  by dashed line, and  $c$  and  $s$  nullclines, labeled  $C_{eq}$  and  $S_{eq}$ , respectively, on VSS by dotted lines.

$(c,s,V)$  space. The dashed line  $HC$  identifies the location of the saddle-node bifurcation in  $(c,s,V)$  space and the nullclines for  $c$  and  $s$  (labeled  $C_{eq}$  and  $S_{eq}$ , respectively) are superimposed on VSS. During the silent phase of the burst cycle, the solution trajectory lies on VSS, and the dynamics collapse to a second order system with Eqs. (1) and (2) at steady state as a function of  $c$  and  $s$ . On crossing  $HC$  (i.e.,  $g_{S1} = g_{HC}$ ) the model begins firing a burst of action potentials as long as the solution trajectory remains on AP ( $g_{S1}$

$> g_{HC}$ ). The burst continues until  $HC$  is again crossed and the solution trajectory relaxes back to VSS ( $g_{S1} < g_{HC}$ ).

A more compact view of the dynamics of the model is illustrated in Fig. 2, which illustrates the solution trajectory of Fig. 1 in  $(c,s)$  space. The dotted lines are the equilibrium nullclines, the dashed line is  $HC$ , and the dash-dotted lines are the averaged nullclines. Each point of an averaged nullcline is a value of  $(c,s)$  where the appropriate equation [Eq. (3) or (4)] averaged over one period of AP is approxi-

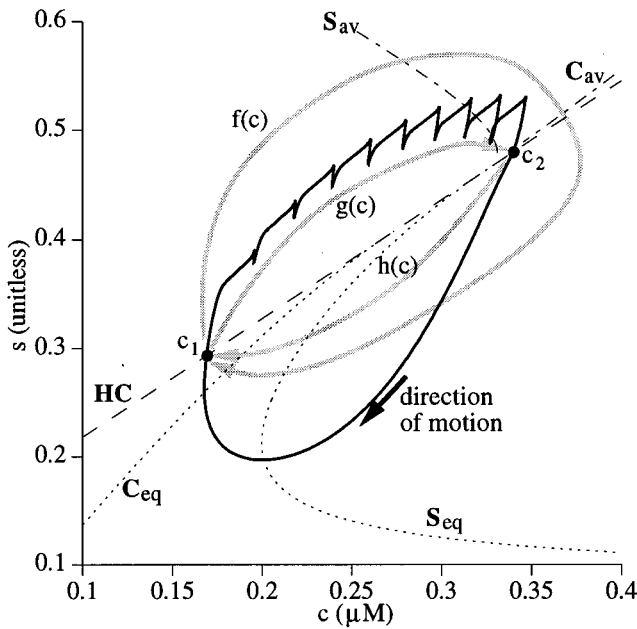


FIG. 2. Origin of first-return maps. Solution trajectory from Fig. 1 displayed in  $(c, s)$ . Also shown are equilibrium nullclines (dotted,  $C_{eq}$  and  $S_{eq}$ ), average nullclines (dash-dotted,  $C_{av}$  and  $S_{av}$ ), and saddle-node bifurcation  $HC$  (dashed). First-return map  $f(c)$  maps crossings of  $HC$  from  $VSS$  to  $AP$  to successive crossings. This map is further decomposed into  $g(c)$  and  $h(c)$ , where  $f(c) = h(g(c))$ . For the limit cycle illustrated  $c_1 = f(c_1)$ ,  $c_2 = g(c_1)$ , and  $c_1 = h(c_2)$ .

mately equal to zero.<sup>23-25</sup> In summary, bursting occurs as the solution trajectory crosses back and forth across  $HC$ . When  $g_{SI} < g_{HC}$ , the model dynamically collapses to a second-order system in  $(c, s)$  which lies on  $VSS$ . When  $g_{SI} > g_{HC}$ , the dynamics are still largely determined by  $c$  and  $s$ , but they are subject to periodic perturbations due to the firing of action potentials. In the classification scheme of bursting neurons,<sup>14,26</sup> our model is a type II burster.

Let  $HC1$  define a set of points along  $HC$  such that  $\partial g_{SI} / \partial t > 0$ . Since  $HC1$  is one dimensional, we may utilize  $c$  as our index along  $HC1$ . It can be shown that there exists a point  $c_p$  such that  $HC1$  is a continuous curve consisting of all points along  $HC$  where  $c < c_p$ . Likewise, let  $HC2$  define points along  $HC$  where  $c > c_p$ . Bursting solution trajectories cross  $HC1$  when crossing from the  $VSS$  to  $AP$  manifold (e.g., point  $c_1$  in Fig. 2). Likewise, bursting solutions cross  $HC2$  when crossing from the  $AP$  to  $VSS$  manifolds (e.g., point  $c_2$  in Fig. 2). Let  $f(c)$  define a one-dimensional map which describes how points along  $HC1$  return to  $HC1$ . This map is generated numerically as follows: The bifurcation analysis of the FAST subsystem provides a numerical estimate of the location of the knee ( $g_{HC}, V_{HC}$ ). For a given value of  $c$ , set the model to the initial conditions  $V = V_{HC}$ ,  $w = w_\infty(V_{HC})$ , and  $s = g_{HC} / \bar{g}_{SI}(1 + \beta c)$ . This is the location in state space of a point along  $HC1$ . Numerically integrate the model until  $HC1$  is again crossed and calculate the value of  $c$  where the solution trajectory returned to  $HC$ . Repeat this process for a range of values of  $c$  along  $HC1$ .

The map  $f(c)$  can be decomposed into two submaps,  $g(c)$  and  $h(c)$ , which describe how points along  $HC1$  map

to  $HC2$  and points along  $HC2$  map to  $HC1$ , respectively. Thus  $f(c) = h(g(c))$ . These maps are obtained by calculating the location in state space where  $HC2$  is crossed when using the above procedure to calculate  $f(c)$ .

There exists a degree of inaccuracy in these mappings. Figure 1(B2) illustrates that the trajectory does not lie exactly on  $VSS$  when the solution trajectory crosses  $g_{HC}$  from  $VSS$  to  $AP$  (i.e.,  $HC1$  is crossed). Even more significantly, when the trajectory crosses  $g_{HC}$  from  $AP$  to  $VSS$  (i.e.,  $HC2$  is crossed), the trajectory does not immediately jump to the equilibrium surface. By modifying the above procedure to allow one complete burst cycle (i.e., successive crossings of  $HC2$  and  $HC1$ ) to occur before calculating the map, most of this error is eliminated, and the maps accurately define periodic bursting solutions. Maps generated in this manner will be denoted  $\tilde{f}(c)$ . The accuracy of these maps were further verified by two additional measures: maps calculated independently from subsequent burst cycles superimposed identically, and second-return maps calculated in a procedure analogous to that just described superimposed identically with numerically iterated first-return maps. The disadvantage of this approach is that the points on the map are confined to the domain of attraction of the bursting solutions and do not allow the entire state space to be sampled evenly. When viewed over a large scale  $f(c)$  and  $\tilde{f}(c)$  are nearly indistinguishable. Thus  $f(c)$  will be used for most mappings shown in this study, while  $\tilde{f}(c)$  will be utilized when the map is examined at a fine scale.

The use of these maps is only appropriate for locating bursting solutions. In many parameter regions a beating solution may coexist. The existence of a stable beating solution may be implied by the existence of regions of discontinuity in  $f(c)$ , i.e., those initial conditions on  $HC1$  that never cross  $HC1$  again. However, such features of  $f(c)$  are not necessary for a stable beating solution to exist, and the existence of such a solution must be verified by alternative means. For example, stability analysis of the intersection of the averaged nullclines is typically sufficient to predict the stability of the beating solution.<sup>25</sup>

## V. RESULTS

### A. From bursting to beating

Canavier *et al.*<sup>2,3</sup> illustrated several pathways from a single bursting limit cycle to a single beating limit cycle as a parameter is varied. These pathways involved varying conductances and or the applied current. Typically, as a parameter was varied, the dynamics progressed from a single stable bursting limit cycle to a multirhythmic state with many coexisting bursting solutions to a single stable beating solution. We have observed similar pathways in our minimal model. For the results shown here we choose  $\tau_s$ , the time constant of the slow variable  $s$ , as our bifurcation parameter. We have chosen this parameter for ease of presentation: The FAST subsystem bifurcation diagram (including the calculation of  $HC$ ) and steady-state solution manifolds  $AP$  and  $VSS$  do not depend on this parameter. Thus the nullclines,  $HC$  and

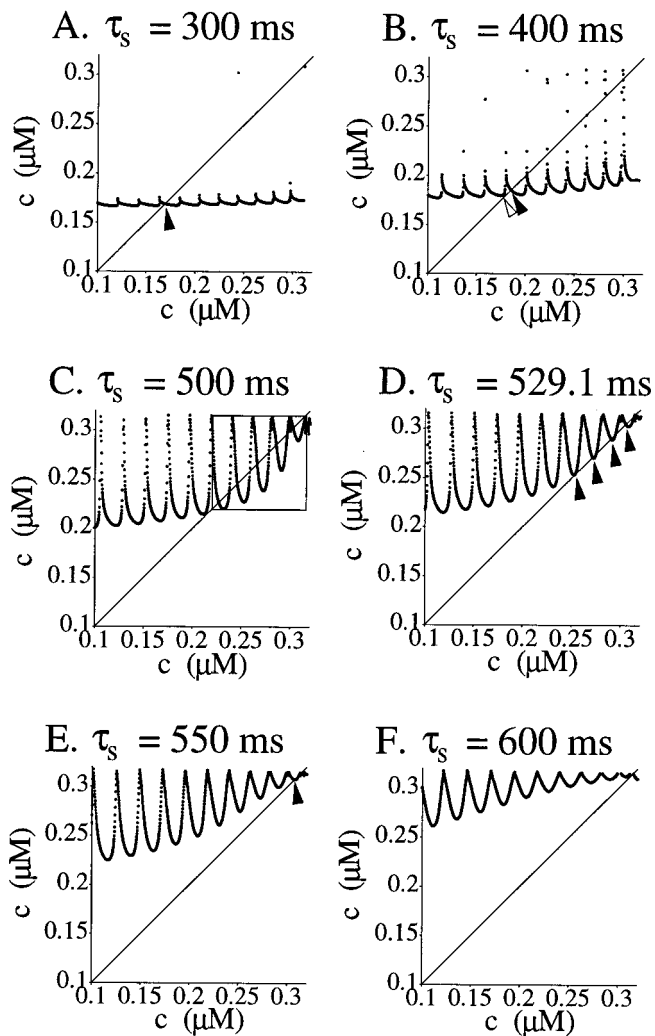


FIG. 3. First-return maps  $f(c)$  for various values of  $\tau_s$ . Solid arrows indicate stable fixed points. See text for description of open arrow.

steady-state solution surfaces shown in Figs. 1(B)–1(C) and 2 are valid for all values of  $\tau_s$ —only the solution trajectories vary with  $\tau_s$ .

Figure 3 illustrates the numerically calculated maps  $f(c)$  for six different values of  $\tau_s$ . Panel (A) illustrates the map obtained using the value of  $\tau_s$  corresponding to the bursting limit cycle solution illustrated in Figs. 1 and 2. This map possesses a single stable fixed point (black arrow) and is relatively flat (i.e., contractive), with most initial conditions converging to the fixed point quickly. The most noticeable feature of the map is that it consists of many apparently discrete, smooth curve segments. Each curve segment is separated by a steep transition region which requires extremely high resolution to map at low values of  $\tau_s$ . Further examination of the data, supported by numerous simulations from a variety of initial conditions, revealed that within each curve segment the first-return trajectory contains an identical number of action potentials. For example, the curve segment containing the fixed point contains all burst trajectories with initial conditions on *HCl* that contain 9 action potentials. The curve segment to the left contains all burst trajectories

with initial conditions on *HCl* that contain 10 action potentials, the curve segment to the right, 8 action potentials.

As  $\tau_s$  is increased from 300 ms, each curve segment comes more U-shaped and  $f(c)$  becomes less flat. Figure (B) illustrates  $f(c)$  when  $\tau_s=400$  ms. This map also has a single stable fixed point (black arrow). This figure elucidates the nature of a transition between limit cycles with  $n$  and  $n+1$  action potentials as a parameter is varied. The stable fixed point in panel (B) corresponds to a limit cycle with 8 action potentials. As  $\tau_s$  is decreased,  $f(c)$  shifts downward [compare with panel (A)]. This downshift in  $f(c)$  increases the slope of  $f(c)$  at the fixed point. A local examination of the map shows that it loses stability via a period-doubling bifurcation. A new stable fixed point emerges (near white row) corresponding to a stable limit cycle solution with 9 action potentials. This solution coexists with the period-2 solution with 8 action potentials. As  $\tau_s$  is further reduced, the period-2 solution with 8 action potentials continues to lose stability via a period-doubling route and eventually disappears. This transition occurs over a narrow range of parameters. However, the general mechanism appears ubiquitous, at least within the context of our model. We have, via numerical simulation, located several parameter regimes where a period-1 bursting limit cycle with  $n+1$  action potentials and a period-2 bursting limit cycle with  $n$  action potentials coexist. We have identified similar transitions between bursting limit cycles of  $n$  and  $n+1$  action potentials as a parameter is varied in the bursting model of Rinzel and Ye.<sup>13</sup>

As  $\tau_s$  is further increased,  $f(c)$  becomes more divergent and the curve segments at higher values of  $c$  rise toward the identity line. In Fig. 3(C), the map consists of only unstable fixed points. There exists a region of the map (indicated by the square box) that is an attractor, i.e., the range of  $f(c)$  is a subset of the domain. Trajectories that enter this region never leave. The solution trajectory consists of successive bursts of anywhere from 2 to 6 action potentials, with the nature of the burst corresponding to which curve segment of  $f(c)$  each iterate (i.e., successive burst cycle) falls on. This is one form of chaotic dynamics exhibited by the model—a chaotic attractor which spans burst trajectories that contain a varying number of action potentials per burst. We refer to this mode of activity as global chaotic bursting.

At a higher value of  $\tau_s$  (515 ms, not shown),  $f(c)$  shifts upward slightly and the fixed point at the lowest value of  $c$  in Fig. 3(C) ( $c \approx 0.225$ ) becomes stable. In this case a stable bursting limit cycle exists, but convergence is quite slow for initial conditions on *HCl* where  $0.225 < c < 0.32$ . We attribute this to the existence of several marginally unstable fixed points in  $f(c)$ . Trajectories with initial conditions in this region may take many cycles (20 or more) before finally converging to the stable bursting limit cycle. We have found parameter regions of the model of Canavier *et al.*<sup>1</sup> that also exhibit this phenomena.

For some parameter values (Fig. 3(D),  $\tau_s=529.1$  ms)  $f(c)$  possesses multiple stable attracting solutions (black arrows). This map will be examined in greater detail shortly. As  $\tau_s$  is further increased,  $f(c)$  starts to contract and the number of fixed points (stable or unstable) decreases, with

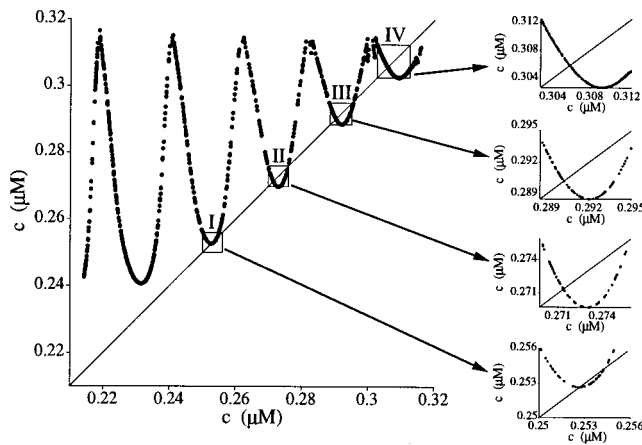


FIG. 4. First-return map  $\tilde{f}(c)$  for  $\tau_s = 529.1$  ms. To the right of the figure are expanded views of the boxed regions I–IV. Each of these regions identifies a corresponding limit cycle in Fig. 5.

most of  $f(c)$  existing above the identity line. In Fig. 3(E), a single burst solution (with two action potentials per burst) exists. Finally, in Fig. 3(F),  $f(c)$  no longer possesses any stable fixed points. A stable beating solution exists at this parameter set, implied by discontinuities in  $f(c)$ .

**B. Multirhythmic solutions**

Figure 4 illustrates the map  $\tilde{f}(c)$  for  $\tau_s = 529.1$  ms. Panels I–IV illustrate closeup views of four regions of  $\tilde{f}(c)$ . Each of these regions corresponds to a stable bursting solution. These four solutions are illustrated in Fig. 5. Panel I of Fig. 4 illustrates a stable fixed point and corresponds to the period-1 solution labeled I in Fig. 5. Panels II–IV do not illustrate regions of  $\tilde{f}(c)$  with stable fixed points. Rather, in each of these panels is illustrated a local region of  $\tilde{f}(c)$

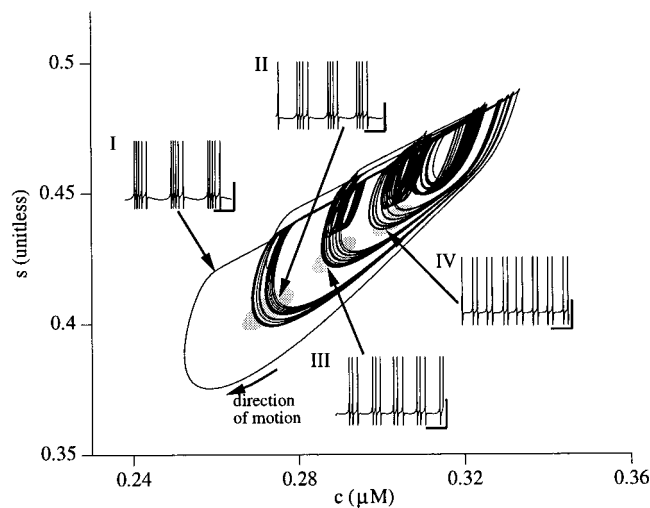


FIG. 5. Multirhythmic bursting. Trajectories I–IV correspond to similar labeled regions of  $\tilde{f}(c)$  in Fig. 4. Trajectories II–IV are chaotic. Insets illustrate time course of membrane potential for each solution. For each inset, the scale bar indicates 2 s and 20 mV.

where the range of  $\tilde{f}(c)$  is a subset of the domain. Each of these regions is reminiscent of an upside-down logistics map and acts as a dynamic equivalent of a “potential well” — once the limit cycle trajectory maps into this region it cannot leave. These attracting regions of the map without stable fixed points suggest chaotic dynamics, illustrated by the corresponding  $(c,s)$  trajectories in Fig. 5. Additional numerical simulations have verified the stability of each of these regions of attraction. While each attractor may appear to have chaotic dynamics, the number of action potentials within each burst is identical from cycle to cycle. This contrasts with the global chaotic bursting described earlier as a result of an attracting region that spanned over several curve segments of  $f(c)$ .

**C. Origin of multirhythmic bursting**

What dynamical features of our bursting model give rise to return maps with multiple stable attractors? The state-space dynamics of the model fall into two regions. When the trajectory lies on  $VSS$ , it is dynamically a second-order system. When the trajectory lies on  $AP$ , the dynamics of the model are still largely determined by  $c$  and  $s$ , subject to perturbations associated with the firing of each action potential. We now decomposed  $f(c)$  into two separate maps,  $g(c)$  and  $h(c)$ , where  $f(c) = h(g(c))$ . Thus  $g(c)$  describes how points on  $HC1$  map to  $HC2$  and  $h(c)$  describes how these trajectories return to  $HC1$  as a function of where they crossed  $HC2$ . Figure 6 illustrates  $g(c)$  and  $h^{-1}(c)$  for each of the corresponding  $f(c)$  maps shown in Fig. 3. In each panel of Fig. 6, the intersections of  $g(c)$  and  $h^{-1}(c)$  correspond to the fixed points illustrated in Fig. 3. We will often refer to the slope of  $h(c)$  in the following paragraphs, even though Fig. 6 illustrates  $h^{-1}(c)$ .

There is a certain degree of inaccuracy in our calculation of  $h(c)$ . Ideally, we would take initial conditions on  $HC2$  and calculate how those trajectories map to  $HC1$ . However, as indicated earlier, on crossing  $HC2$  the solution trajectory does not instantaneously jump from  $AP$  to  $VSS$ . For this reason we have calculated  $h(c)$  as described earlier, so that  $g(c)$  and  $h(c)$  truly represent a decomposition of  $f(c)$  that was calculated numerically.

The segmentation of  $f(c)$  is evident in the segmentation of  $g(c)$  as well. Each curve segment of  $g(c)$  corresponds to those paths from  $HC1$  to  $HC2$  that contain an identical number of action potentials. However, unlike  $f(c)$ , as  $\tau_s$  is increased, there is little change in the shape of  $g(c)$ . As  $\tau_s$  is increased,  $g(c)$  actually becomes more contractive, contrary to the change in  $f(c)$ . The map  $h(c)$  undergoes a significant change in shape as  $\tau_s$  is increased. When  $\tau_s = 300$  ms [panel (A)],  $h(c)$  is very contractive — most initial conditions on  $HC2$  map to a narrow region of  $HC1$ . In this case the segmentation of  $g(c)$  is irrelevant, since  $h(c)$  maps most points on  $HC2$  to a single curve segment of  $HC1$ , and only a single stable limit cycle exists. As  $\tau_s$  is increased,  $h(c)$  becomes more dispersive and the dispersive region of  $h(c)$  (where its slope is steep) shifts toward higher values of  $c$ . Thus, as  $\tau_s$  is varied,  $h(c)$  effectively sweeps across  $g(c)$ . The interaction of these two functions gives rise to the complex maps illus-

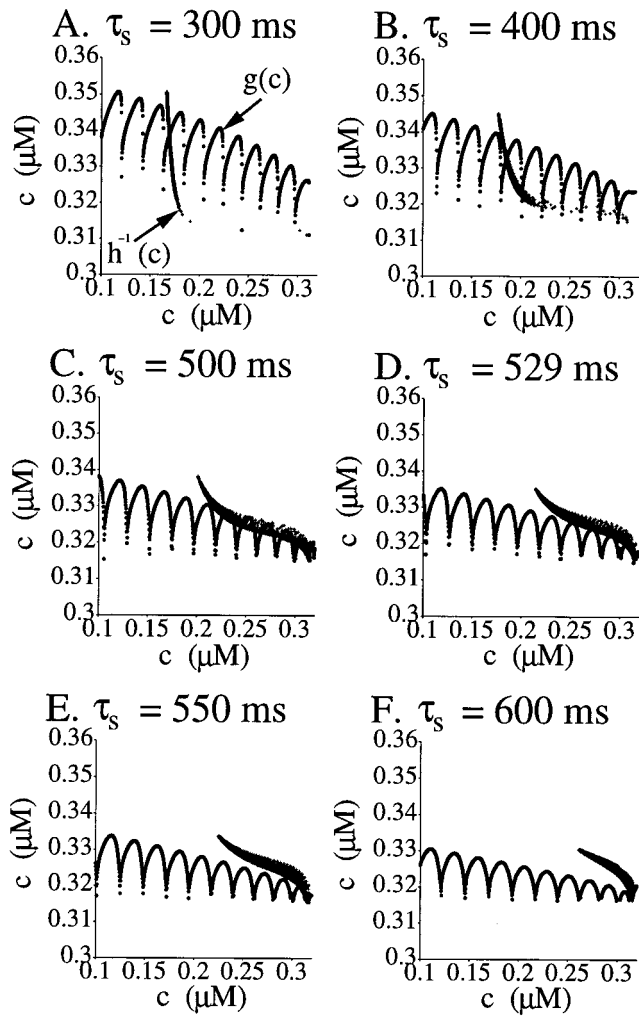


FIG. 6. Decomposed first-return maps for various values of  $\tau_s$ .  $g(c)$  and  $h(c)^{-1}$  are illustrated for each parameter value. See the text for details on the calculation of  $g(c)$  and  $h(c)$ .

trated in Figs. 3(C) and 3(D). As  $\tau_s$  is further increased,  $h(c)$  continues to shift towards higher values of  $c$ , reducing the number of intersections with  $g(c)$  [and thus the number of fixed points of  $f(c)$ ].

It is possible to do an exhaustive examination of the flow field of  $(c,s)$  to more rigorously determine the nature of  $g(c)$  and  $h(c)$ . However, the results up to this point allow us to postulate several sufficient criteria for a bursting model to be capable of exhibiting multirhythmic solutions of the type described here and in Canavier *et al.*<sup>2,3</sup>

(1) *The system must have two slow variables.* In models with a single slow variable bursting arises by coupling the slow variable to a bistable FAST subsystem. Hysteresis is employed so that the solution trajectory alternates between the equilibrium solution branch and the periodic solution branch of FAST. In such bursting models with a single slow variable, the burst typically begins and ends at specific values of the slow variable.<sup>22</sup> In our minimal model the burst begins and ends at a specific value of  $g_{SI}$

defined by a combination of two slow variables. Thus there is a continuum of values of  $(c,s)$  (i.e.,  $HC$ ) where the burst may begin or end.

- (2) *Each action potential has a discrete and sizable effect on one or more of the slow variables.* More generally, the dynamics of the fast variables happen on such a fast time scale that their effects on one or more of the slow variables appear as discrete impulse-like events.
- (3) *A single burst should not have "too many" action potentials.* This concept is model dependent. Criteria 2 and 3 gives rise to a situation where the dynamics of the system in the space of the slow variables is not accurately predicted by simply averaging the effects of the action potentials on the slow variables.<sup>24</sup> These two criteria cause the noticeable segmentation of  $g(c)$ .
- (4) *The dynamics of the slow variables on VSS should not converge to a strongly attracting limit cycle.* Many modeled bursting systems are constructed by adding a fast process (i.e., action potentials) to a slowly varying limit cycle.<sup>16,27</sup> In such models, the solution trajectory during the silent phase of the burst cycle converges to the limit cycle solution that exists in the absence of action potentials (i.e.,  $g_{Na}=0$ ). However, in such situations we would expect  $h(c)$  to be highly contractive, as all initial conditions on  $HC2$  would converge to the limit cycle of the subthreshold oscillation during the silent phase of the bursting limit cycle. If  $h(c)$  is strongly contractive then, as illustrated in Fig. 6(A), only a single limit cycle will exist. In both our model and the model of Canavier *et al.*<sup>1</sup> multirhythmic bursting solutions exist at parameter ranges where a subthreshold oscillation does not persist when  $I_{Na}$  is removed from the model.

#### D. A general model

We sought to implement the above criteria in the simplest possible dynamical system. Our model consists of three variables. The two slow variables  $x$  and  $y$  form a second-order underdamped linear system. The only fixed point of the second-order system is a fixed point at the origin that behaves as a weakly stable focus. This system is coupled to a fast phase variable  $\theta$  defined over the range  $0$  to  $2\pi$ . The dynamics of this variable are dependent on  $y$ . When  $y < 0$ ,  $\theta$  converges toward a stable fixed point. When  $y > 0$ ,  $\theta$  increases at a rate that is dependent on  $y$ . When  $\theta$  passes through a critical value  $\theta_{crit}$ , it feeds back onto  $x$  and  $y$  via a Dirac delta function to perturb  $x$  and  $y$ . The formulation of  $\theta$  is similar to that presented in Baer *et al.*<sup>24</sup> The complete set of equations for the general model is:

$$\dot{\theta} = \omega_f (1 - \cos(\theta) + y), \quad (6)$$

$$\dot{x} = \alpha x + \beta y + \delta(\theta - \theta_{crit}) r_p \cos(\theta_p), \quad (7)$$

$$\dot{y} = -\beta x - \alpha y + \delta(\theta - \theta_{crit}) r_p \sin(\theta_p), \quad (8)$$

where  $\delta$  is the Dirac delta function and  $\alpha = 0.03$ ,  $\beta = 1$ ,  $\omega_f = 25$ ,  $\theta_{crit} = \pi/2$ ,  $r_p = 0.1$ , and  $\theta_p = \pi/72$ . Compared to our minimal bursting model,  $y = 0$  is analogous to  $HC$ . Just as the frequency of firing of our FAST system starts at zero and increases as  $g_{SI}$  is advanced past  $g_{HC}$ , the frequency of  $\theta$  is

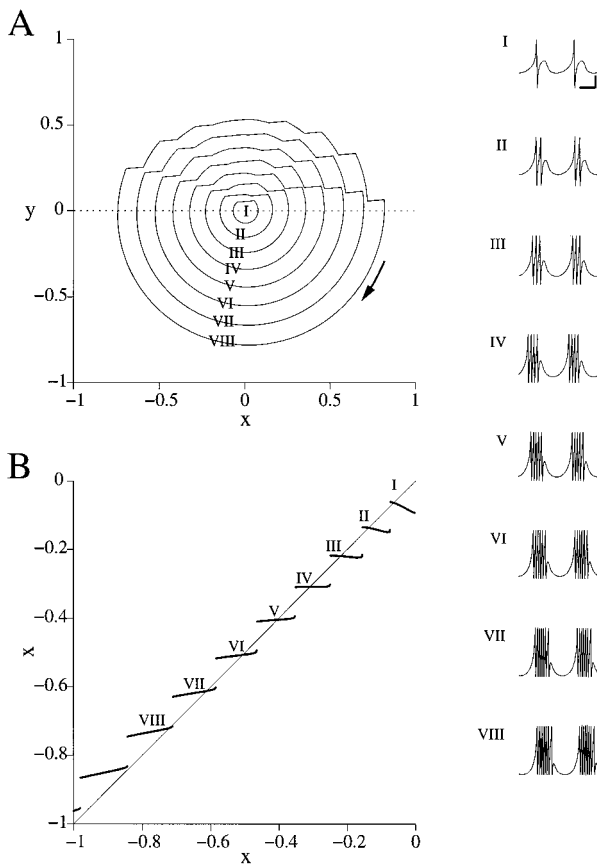


FIG. 7. An idealistic model of multirhythmic bursting. (A). Solution trajectories of eight coexisting bursting solutions in the phase space of the two slow variables  $x$  and  $y$ . Panels I–VIII illustrate the time course of  $\sin(\theta)$  for the corresponding solutions in panel (A). (B). First-return map obtained by using positive crossings of  $y=0$  as a Poincaré section. The scale bar in panel VIII indicates 2 s and 0.5 (unitless) and is valid for panels I–VIII.

initially 0 and increases as  $y$  is advanced past 0. The parameters  $r_p$  and  $\theta_p$  describe the effect of each perturbation on the  $x$  and  $y$  variables.

Figure 7(A) illustrates the dynamics of the above system in  $(x, y)$  using the above parameter set. When numerically integrating the above system, care was taken to not integrate the solution trajectory across time points where the Dirac delta functions are triggered. The general model possesses 8 coexisting bursting solutions, labeled I–VIII. The smaller panels at the right of Fig. 7 illustrate the temporal nature of each solution trajectory by plotting  $\sin(\theta)$  vs time. Figure 7(B) illustrates a numerically calculated first-return map. This map was calculated by choosing as a Poincaré section positive crossings of  $y=0$  and is analogous to the maps  $f(c)$  calculated for our minimal model.

### E. A complex biophysical model

We wished to apply the techniques used to calculate  $f(c)$  to the model of Canavier *et al.*,<sup>1</sup> a much more complex model with 11 state variables. The mechanism of bursting in their model is based on two slow variables  $c$  and  $s$  which modulate a slow-inward  $\text{Ca}^{2+}$  current similar to that presented in our minimal model. A FAST–SLOW analysis similar to that described in Section IV was performed on a

variation of the model of Canavier *et al.*<sup>1</sup> This model<sup>7</sup> possesses a state space geometry<sup>28</sup> similar to the minimal model presented in this paper, with the key differences between the two models described below. Furthermore, we have determined that the state-space of the model of Butera *et al.*<sup>7</sup> is geometrically similar to the model of Canavier *et al.*<sup>1</sup> (unpublished observations).

The analysis of our minimal model exploited the fact that the two slow variables combined to parametrize the system of fast variables in a single functional expression. This single quantity defined the location of  $HC$  in  $(c, s)$  and was used as our Poincaré section. Unfortunately, the model of Canavier *et al.*<sup>1</sup> has several other currents (for example, a  $\text{Ca}^{2+}$ -extrusion pump and a  $\text{Na}^{+}$ - $\text{Ca}^{2+}$  exchanger) which are also dependent on the slow variable  $c$ . In this case  $HC$  cannot be expressed by a single functional expression of  $c$  and  $s$  and must be numerically calculated at any given value of  $(c, s)$ . Such a calculation is quite possible, but utilizing this numerically calculated curve as a Poincaré section in  $(c, s)$  is much more tedious. However,  $HC$  is nearly isopotential, varying only by a few mV across the dynamic range of  $c$  and  $s$ . Thus we defined our Poincaré section as positive crossings of a predefined membrane potential  $V_c$ , where  $V_c$  is a value close to but less than the minimal value of  $HC$  (in  $V$ ) over the dynamics range of  $(c, s)$  to be investigated. Initial conditions were chosen along the line formed by the intersection of the plane  $V_c$  with the surface  $VSS$ . These were calculated for a given value of  $c$  by setting  $V$  to  $V_c$ , all other variables except  $s$  to their steady-state values (which are defined in terms of  $V$  and  $c$ ) and  $s$  to the value necessary to ensure that  $\dot{V}=0$  (the definition of points on  $VSS$ ). Parameters of the model were set identical to those used to generate Fig. 2 of Ref. 2.

The maps  $f(c)$  were much less accurate at indicating the dynamic activity of the model than the maps calculated using our minimal model. This is due to several reasons. First, the model of Canavier *et al.*<sup>1</sup> possesses a coexisting beating solution, so for some initial conditions the solution trajectory never crossed the Poincaré section again. Second, it was necessary to adopt an ad-hoc criterion based on the value of  $dV/dt$  to determine if crossings of  $V_c$  were due to the beginning of a burst or successive firings of action potentials during the burst. Third, their model possesses two additional “slow” state variables that are only active during the firing of action potentials and decay (on a faster time scale) back to steady-state values during the interburst interval. As before these problems were alleviated by using the second burst cycle from each initial condition to define the approximate first-return map  $\tilde{f}(c)$ . The accuracy of these maps was verified by comparing the second-return map obtained by iterating  $\tilde{f}(c)$  with the second-return map obtained analogous to the procedure just described.

Figure 8 illustrates the periodic burst solutions in  $(c, s)$ . These solutions are labeled in a similar manner as Fig. 2 of Ref. 2. The map  $\tilde{f}(c)$  is shown in Fig. 8(B). Regions of  $\tilde{f}(c)$  enclosed by a box predict the bursting solutions in panel A and are shown as expanded insets at the right of the figure. In the insets,  $\tilde{f}(c)$  is represented by circles and  $\tilde{f}^2(c)$

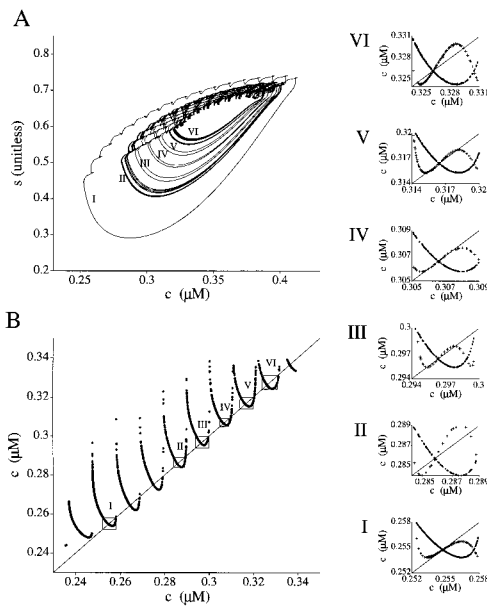


FIG. 8. Multirhythmic bursting in the model of Canavier *et al.* (Refs. 1 and 2) (A). Six co-existing bursting solutions in the phase space of the two slow variables  $c$  and  $s$ . Similar to Fig. 2 of Canavier *et al.* (Ref. 2). (B). First-return map  $\tilde{f}(c)$  for the same parameter set. Boxed insets are blown up at right and correspond to the similarly labeled solution trajectories in panel (A). In the insets  $\tilde{f}(c)$  is indicated by circles and  $\tilde{f}^2(c)$  by plus signs.

by plus signs. The most striking feature of  $\tilde{f}(c)$  is that it is qualitatively similar in shape to Fig. 4, although the number of curve segments which cross the identity line is even larger. Each of the insets identifies mappings which are consistent with the observed limit cycles shown in panel (A). Trajectory I is a stable limit cycle and corresponds to a stable fixed point of  $\tilde{f}(c)$ . Trajectories III, IV, and V are period-2 solutions. The corresponding insets reveal that each of these solutions is confined to a region of  $\tilde{f}(c)$  where the fixed point is marginally unstable, having recently undergone a period-doubling bifurcation. The second return maps  $\tilde{f}^2(c)$  each possess two stable fixed points identifying the period-2 solutions. The chaotic trajectories II and VI correspond to regions of  $\tilde{f}(c)$  where the fixed points are unstable but the mapping  $\tilde{f}(c)$  possesses an attracting region where the range of  $\tilde{f}(c)$  is a subset of the domain. The two curve segments between solutions I and II contain neither fixed points nor stable attracting regions.

Our indirect approach for estimating  $f(c)$  with the model of Canavier *et al.*<sup>1</sup> may not find every possible bursting solution. Since our algorithm is based only on membrane potential, it is necessary to determine the end of a burst so that the following positive crossing of  $V_c$  is known to indicate the beginning of a new burst cycle. Whether a negative crossing of  $V_c$  is the repolarization of an action potential or the hyperpolarizing phase of the depolarizing after-potential (DAP, which occurs at the end of each burst) is determined by the value of  $dV/dt$  at the time of the crossing. If  $V_c$  is set too high, it is possible that the DAP never crosses it. If  $V_c$  is too low, it is possible that some burst trajectories in their silent phase do not hyperpolarize below  $V_c$ . Canavier *et al.*<sup>3</sup>

identified an additional bursting solution with the parameter set studied in this paper which was not located by our algorithm. None of these issues is a problem in our minimal membrane model, which clearly identifies the beginning and end of each burst by positive and negative crossings of  $g_{HC}$ , which are easily calculated in terms of  $c$  and  $s$ .

## VI. DISCUSSION

In this study we have investigated multirhythmic bursting in a minimal membrane model. From those results, we proposed qualitative mechanisms that may combine to contribute to this multistability and tested those mechanisms in a general three-variable model. Finally, we demonstrated that the multistable solutions exhibited by our membrane model appear similar to those of the more complex model of Canavier *et al.*<sup>1</sup> In both models the multistable bursting solutions are nested in the state space of the slow variables and differ by the number of action potentials in their limit cycles. Both models also possess similar maps  $\tilde{f}(c)$ .

One difference between the  $f(c)$ 's calculated from both membrane models and the general model is the shape of each curve segment. For the membrane models they are U-shaped: initial conditions at each end of a curve segment map to similar regions. The curve segments calculated for our general model are more linear, although they do appear to round up at the positive end of each segment. Quite certainly our general model loses a bit of both complexity and realism by approximating the perturbational affects of the action potentials as discrete perturbations. Terman<sup>29</sup> has performed a detailed analysis of the transition between bursts of  $n$  and  $n + 1$  action potentials in a bursting model with a single slow variable. It is possible that a variation of his approach may shed some light on the nature of shape of each curve segment.

It would be quite difficult to identify multistable bursting in a real biological preparations. Our results show that this is a transitional phenomenon in the parameter space between bursting and beating, and immediately adjacent to multistable regions in parameter space may be regions where no stable solution trajectories exist and the bursting is chaotic. However, the multistable solutions are surrounded in parameter space by larger regions where  $f(c)$  is still complex. In these regions  $f(c)$  has a similar shape and suggests that convergence to a stable limit cycle, if one exists, may take many limit cycles. Our data reveal (not shown) that the length of each burst cycle is somewhat determined by which curve segment of  $f(c)$  the current cycle started from. Thus it may be possible to construct a map with a structure similar to  $f(c)$  by biasing the neuron to a regime of irregular burst firing. In our model, the structure of such maps was most evident when plotting the duration of each interburst interval versus the duration of the interburst interval of the previous cycle. However, given the inherent variability of biological preparations, the data may not unambiguously reveal any structure in such a map. An even simpler approach would be to employ the method of symbolic dynamics<sup>30,31</sup> to analyze a bursting time series for recurring patterns. In such an approach, the number of action potentials in each burst is as-

signed a symbol. A time series of burst cycles is converted to a string of symbols denoting the number of action potentials in each burst. An examination of words (substrings of successive symbols) may reveal common words or forbidden words. For example, it is evident from Fig. 4 that a burst of  $n$  action potentials ( $2 \leq n \leq 5$ ) may only be followed by a burst of 2 to  $\min(n+1, 5)$  action potentials. Similar structures may be apparent in experimental recordings.

Even if such multistability was identified in a biological preparation, it would be a subject of great speculation how a nervous system would exploit such a feature. However, the features identified in this study could be exploited for man-made applications. Alternative formulations of our general model [primarily Eq. (6)] give rise to systems which would be amenable to analytical treatment. These near-linear systems could be easily implemented with existing integrated circuit components. It may be possible to design oscillatory circuits that have many more than the 8 stable limit cycles demonstrated in our general model. Unlike chaotic attractors, which are often described as an infinite collection of unstable periodic solutions, these circuits would have a finite number of periodic solutions. Such circuits could possibly have applications in communications<sup>32</sup> (e.g., the encoding/decoding circuits could choose from multiple coexisting chaotic oscillations) or as a novel form of dynamic memory.<sup>33,34</sup> To date, multistable systems based on delayed feedback have been constructed from both optical<sup>33-35</sup> and digital<sup>36</sup> components.<sup>19</sup>

## ACKNOWLEDGMENTS

I wish to thank Gerda de Vries and John Rinzel for critical readings of the manuscript, and Artie Sherman for helpful discussions, and the referees for their helpful comments.

## APPENDIX: Model Description

The following equations define the equations and parameters functions referenced in Eqs. (1)–(4).

### 1. Equations

$$I_{Na}(V) = \bar{g}_{Na} m_{\infty}(V)(V - E_{Na}),$$

$$m_{\infty}(V) = \frac{1}{2}(1 + \tanh((V - a_m)/b_m)),$$

$$I_K(V, w) = \bar{g}_K w(V - E_K),$$

$$w_{\infty}(V) = \frac{1}{2}(1 + \tanh((V - a_w)/b_w)),$$

$$\tau_w(V) = 1/\cosh((V - a_w)/(2b_w)),$$

$$I_{SI}(V, c, s) = g_{SI}(c, s)(V - E_{Ca}),$$

$$g_{SI}(c, s) = \frac{\bar{g}_{SI} s}{1 + \beta c},$$

$$s_{\infty}(V) = \frac{1}{2}(1 + \tanh((V - a_s)/b_s)),$$

$$I_L(V) = \bar{g}_L(V - E_K).$$

## 2. Parameters and units

Time is in ms, membrane potential in mV, concentration in  $\mu\text{M}$ , and gating variables are unitless. Current and conductances are normalized to cell capacitance and thus have the units  $\text{mV}/\text{ms}$  and  $\text{ms}^{-1}$ , respectively. All other parameters are expressed in terms of these quantities. The value of  $\tau_s$  is specified in the text for each simulation:

$$\bar{g}_{Na} = 0.2 \text{ V/s}, \bar{g}_K = 0.4 \text{ V/s}, \bar{g}_{SI} = 0.05 \text{ V/s}, \bar{g}_L = 0.1 \text{ V/s}, \\ E_{Na} = 55 \text{ mV}, E_K = -75 \text{ mV}, E_{Ca} = 120 \text{ mV}, a_m = -25 \text{ mV}, \\ a_w = -20 \text{ mV}, a_s = -45 \text{ mV}, b_m = 14 \text{ mV}, b_w = 10 \text{ mV}, b_s \\ = 15 \text{ mV}, \beta = 10.0 \mu\text{M}^{-1}, I_{STIM} = 1.1 \text{ V/s}, k_{Na} = 1.2 \times 10^{-4} \\ \mu\text{M}/\text{mV}, k_{SI} = 2.5 \times 10^{-5} \mu\text{M}/\text{mV}, k_c = 5 \times 10^{-5} \text{ ms}^{-1}$$

- <sup>1</sup> C. C. Canavier, J. W. Clark, and J. H. Byrne, "Simulation of the bursting activity of neuron R15 in *Aplysia*: Role of ionic currents, calcium balance, and modulatory transmitters," *J. Neurophysiol.* **66**, 2107–2124 (1991).
- <sup>2</sup> C. C. Canavier, D. A. Baxter, J. W. Clark, and J. H. Byrne, "Nonlinear dynamics in a model neuron provide a novel mechanism for transient synaptic inputs to produce long-term alterations of post-synaptic activity," *J. Neurophysiol.* **69**, 2252–2257 (1993).
- <sup>3</sup> C. C. Canavier, J. W. Clark, D. A. Baxter, and J. H. Clark, D. A. Baxter, and J. H. Byrne, "Multiple modes of activity in a model neuron suggest a novel mechanism for the effects of neuromodulators," *J. Neurophysiol.* **72**, 872–882 (1994).
- <sup>4</sup> H. A. Lechner, D. A. Baxter, J. W. Clark, and J. H. Byrne, "Bistability and its regulation by serotonin in the endogenously bursting neuron R15 in *Aplysia*," *J. Neurophysiol.* **75**, 957–962 (1996).
- <sup>5</sup> E. Marder, L. F. Abbott, G. G. Turrigiano, Z. Liu, and J. Golowasch, "Memory from the dynamics of intrinsic membrane currents," *Proc. Natl. Acad. Sci. USA* **93**, 13481–13486 (1996).
- <sup>6</sup> J. Hounsgaard and O. Kiehn, "Serotonin-induced bistability of turtle motoneurons caused by a nifedipine-sensitive calcium plateau potential," *J. Physiol. (London)* **414**, 265–282 (1989).
- <sup>7</sup> R. J. Butera, J. W. Clark, C. C. Canavier, D. A. Baxter, and J. H. Byrne, "Analysis of the effects of modulatory agents on a modeled bursting neuron: Dynamic interactions between voltage and calcium dependent systems," *J. Comput. Neurosci.* **2**, 19–44 (1995).
- <sup>8</sup> V. Booth and J. Rinzel, "A minimal, compartmental model for a dendritic origin of bistability of motoneuron firing patterns," *J. Comput. Neurosci.* **2**, 299–312 (1995).
- <sup>9</sup> A. Goldbeter, *Biochemical Oscillations and Cellular Rhythms* (Cambridge University Press, Cambridge, 1996).
- <sup>10</sup> This is partially due to the role of the subcritical Hopf bifurcation in many neuronal models. See for example Ref. 36.
- <sup>11</sup> O. Decroly and A. Goldbeter, "Selection between multiple periodic regimes in a biochemical system: Complex dynamic behaviour resolved by use of one-dimensional maps," *J. Theor. Biol.* **113**, 649–671 (1985).
- <sup>12</sup> J. Foss, A. Longtin, B. Mensour, and J. Milton, "Multistability and delayed recurrent loops," *Phys. Rev. Lett.* **76**, 708–711 (1996).
- <sup>13</sup> J. Rinzel and Y. S. Lee, "Dissection of a model for neuronal parabolic bursting," *J. Math. Biol.* **25**, 653–675 (1987).
- <sup>14</sup> R. Bertram, M. J. Butte, T. Kiemel, and A. Sherman, "Topological and phenomenological classification of bursting oscillations," *Bull. Math. Biol.* **57**, 413–439 (1995).
- <sup>15</sup> R. Bertram, "A computational study of the effects of serotonin on a molluscan burster neuron," *Biol. Cybern.* **69**, 257–267 (1993).
- <sup>16</sup> R. E. Plant and M. Kim, "Mathematical description of a bursting pacemaker neuron by a modification of the Hodgkin-Huxley equations," *Biophys. J.* **16**, 227–244 (1976).
- <sup>17</sup> W. B. Adams and J. A. Benson, "The generation and modulation of endogenous rhythmicity in the *Aplysia* bursting pacemaker neurone R15," *Prog. Biophys. Mol. Biol.* **46**, 1–49 (1985).
- <sup>18</sup> C. Morris and H. Lecar, "Voltage oscillations in the barnacle muscle fiber," *Biophys. J.* **35**, 193–213 (1981).
- <sup>19</sup> J. Rinzel and G. B. Ermentrout, "Analysis of neural excitability and oscillations," *Methods in Neuronal Modeling*, edited by C. Koch and I. Segev (MIT Press, Cambridge, 1989), Chap. 5, pp. 135–169.
- <sup>20</sup> S. D. Cohen and A. C. Hindmarsh, "Scientific programming CVODE, a stiff/nonstiff ODE solver in C," *Comput. Phys.* **10**, 138 (1996).
- <sup>21</sup> E. J. Doedel, "AUTO: A program for the automatic bifurcation and analysis

- of autonomous systems," *Congr. Numerantium* **30**, 265–284 (1981).
- <sup>22</sup>J. Rinzel, "Bursting oscillations in an excitable membrane model," edited by B. D. Sleeman and D. Jones, *Ordinary and Partial Differential Equations*, Lecture Notes in Mathematics, Vol. 1151 (Springer-Verlag, Berlin, 1985), pp. 304–316.
- <sup>23</sup>P. Smolen, D. Terman, and J. Rinzel, "Properties of a bursting model with two slow inhibitory variables," *SIAM (Soc. Ind. Appl. Math.) J. Appl. Math.* **53**, 861–892 (1993).
- <sup>24</sup>S. M. Baer, J. Rinzel, and H. Carrillo, "Analysis of an autonomous phase model for neuronal parabolic bursting," *J. Math. Biol.* **33**, 309–333 (1995).
- <sup>25</sup>R. J. Butera, J. W. Clark, and J. H. Byrne, "Transient responses of a modeled bursting neuron: Analysis with equilibrium and averaged nullclines," *Biol. Cybern* **77**, 307–322 (1997).
- <sup>26</sup>J. Rinzel, "A formal classification of bursting mechanisms in excitable systems," *Mathematical Topics in Population Biology, Morphogenesis, and Neurosciences*, edited by E. Teramoto and M. Yamaguti, Lecture Notes in Biomathematics (Springer-Verlag, Berlin, 1987), pp. 267–281.
- <sup>27</sup>R. E. Plant and M. Kim, "On the mechanism underlying bursting in the Aplysia abdominal ganglion R15 cell," *Math. Biosci.* **26**, 357–375 (1975).
- <sup>28</sup>R. J. Butera, J. W. Clark, and J. H. Byrne, "Dissection and reduction of a modeled bursting neuron," *J. Comput. Neurosci.* **3**, 199–223 (1996).
- <sup>29</sup>D. Terman, "Chaotic spikes arising from a model of bursting in excitable membranes," *SIAM (Soc. Ind. Appl. Math.) J. Appl. Math.* **51**, 1418–1450 (1991).
- <sup>30</sup>V. Daniels, M. Vallieres, and J.-M. Yuan, "Chaotic scattering on a double-well: Periodic orbits, symbolic dynamics, and scaling," *Chaos* **3**, 475–485 (1993).
- <sup>31</sup>H.-P. Fang and B.-L. Hao, "Symbolic dynamics of the Lorenz equations," *Chaos Solitons Fractals* **7**, 217–246 (1996).
- <sup>32</sup>L. M. Pecora and T. L. Carroll, "Synchronization in chaotic systems," *Phys. Rev. Lett.* **64**, 821–824 (1990).
- <sup>33</sup>T. Aida and P. Davis, "Storage of optical pulse data sequences in loop memory using multistable oscillations," *Electron. Lett.* **27**, 1544–1546 (1991).
- <sup>34</sup>T. Aida and P. Davis, "Oscillation modes of laser diode pumped hybrid bistable system with large delay and application to dynamical memory," *IEEE J. Quantum Electron.* **28**, 686–699 (1992).
- <sup>35</sup>T. Aida and P. Davis, "Oscillation mode selection using bifurcation of chaotic mode transitions in a nonlinear ring resonator," *IEEE J. Quantum Electron.* **30**, 2986–2997 (1994).
- <sup>36</sup>T. Aida, N. Otani, and P. Davis, "Digital implementation of a nonlinear delayed-feedback system," *IEEE Trans. Circuits Syst. I* **41**, 238–242 (1994).